An estimation of the $^{18}O/^{16}O$ ratio of UT/LMS ozone based on artefact CO in air sampled during CARIBIC flights

S. Gromov[1], C. A. M. Brenninkmeijer[1]

[1] Max Planck Institute for Chemistry, Mainz, Germany

Correspondence to: S. Gromov (sergey.gromov@mpic.de)

Abstract

An issue of O_3-driven artefact production of CO in the UT/LMS air analysed in the CARIBIC−1 project is being discussed. By confronting the CO mixing/isotope ratios obtained from different analytical instrumentation, we (i) Reject natural/artificial sampling and mixing effects as possible culprits of the problem, (ii) Ascertain the photochemical nature and quantify the strength of the effect in a general contamination kinetic framework, and (iii) Demonstrate the successful application of the isotope mass-balance calculations for inferring the isotope signature of the contamination source. The $^{18}O/^{16}O$ ratios of the latter unambiguously indicate the oxygen being inherited from O_3. The $^{13}C/^{12}C$ ratios hint at reactions of trace amounts of organics with ample stratospheric O_3 that could have yielded the artificial CO. While the exact contamination mechanism is not known, it is clear that the issue pertains only to the earlier (first) phase of the CARIBIC project. Finally, estimated UT/LMS ozone $^{18}O/^{16}O$ ratios are lower than those observed in the LMS within the same temperature range, suggesting that higher pressures (240−270 hPa) imply lower isotope fractionation controlling the local $\delta^{18}O(O_3)$ value.

1 Introduction

[1] Successful determination of the atmospheric carbon monoxide (CO) content based on the collection of air samples depends on the preservation of the mixing ratio of CO inside the receptacle, from the point of sampling to the moment of physiochemical analysis in a laboratory. A well known example in our field of research is the filling of pairs of glass flasks at South Pole

Station for analysis at NOAA in Boulder, Colorado, USA (Novelli *et al.*, 1998). There, the duplicate air sampling allowed for a degree of quality control which in view of the long transit times, especially during polar winter, was a perhaps not perfect, but certainly a practical measure. Here we deal with a different case: Using aircraft-based collection of very large air samples rendered duplicate sampling unpractical, yet analyses could be performed soon after the sampling had taken place because of the proximity of the aircraft's landing location to the laboratory involved. A presumption of the analytical integrity of the process was that the growth of CO in receptacles is gradual and takes its time. Reminding Thomas Henry Huxley's statement, "The great tragedy of Science – the slaying of a beautiful hypothesis by an ugly fact", it turned out, however, that for air we collected in stainless steel tanks in the upper troposphere/lowermost stratosphere (UT/LMS) higher CO values were measured in the laboratory than measured *in situ* during the collection of these air samples. Moreover, measurement of the stable oxygen isotopic composition of CO from these tanks revealed additional isotopic enrichments in ^{18}O of 10‰ or more. It was soon realised that this phenomenon was due to the formation of CO in these tanks and/or possibly in the sampling system and inlet tubing used, by reactions involving ozone (Brenninkmeijer *et al.*, 1999).

[2] Unexpectedly high $^{18}O/^{16}O$ ratios in stratospheric ozone (O_3) were discovered by Konrad Mauersberger using a balloon-borne mass spectrometer (Mauersberger, 1981), which has triggered a series of theoretical and experimental studies on atmospheric O_3 heavy isotope enrichments (see, *e.g.*, Schinke *et al.* (2006) for a review). In view of the advances in theoretical and laboratory studies on the isotopic composition of O_3 atmospheric measurements are welcome, they do however form a challenge. In the stratosphere O_3 is abundant, but the remoteness of the sampling domain is a problem. In the troposphere, low O_3 concentrations are the main obstacle, as indicated by few experiments performed to date (Krankowsky *et al.*, 1995; Johnston and Thiemens, 1997; Vicars and Savarino, 2014). Nevertheless, recent analytical improvements, namely the use of an indirect method of reacting atmospheric O_3 with a substrate that can be analysed for the isotopic composition of the O_3-derived oxygen (Vicars *et al.*, 2012), has greatly improved our ability to obtain information on the O_3 isotopic composition.

[3] Although the increase of CO concentrations in air stored in vessels is a well recognised problem, to our knowledge a specific O_3-related process has not been reported yet. Here we discuss this phenomenon and turn its disadvantage into an advantage, namely that of obtaining a valid estimate of the oxygen isotopic composition of O_3 in the UT/LMS, an atmospheric domain not yet covered by specific measurements. The air samples we examine in this study were

collected onboard a passenger aircraft carrying an airfreight container with analytical and air/aerosol sampling equipment on long distance flights from Germany to South India and the Caribbean within the framework of the CARIBIC project (Civil Aircraft for the Regular Investigation of the atmosphere Based on an Instrument Container, http://www.caribic-atmospheric.com).

2 Experimental and results

2.1 Whole air sampling

[4] CARIBIC−1 (Phase #1, abbreviated hereafter "C1") was operational from November 1998 until April 2002 using a *Boeing* 767-300 ER operated by LTU International Airlines (Brenninkmeijer *et al.*, 1999). Using a whole air sample (WAS) collection system, twelve air samples were collected per flight (of 8−10 hours duration at cruise altitudes of 10−12 km) in stainless steel tanks for subsequent laboratory analysis of the abundances of various trace gases, including ^{14}CO. Large air samples were required in view of the ultra-low abundance of this mainly cosmogenic tracer (10−100 molecules cm^{-3} STP, about 40−400 amol/mol). (Hereinafter STP denotes dry air at 273.15 K, 101325 Pa.) Each C1 WAS sample (holding 350 litres of air STP) was collected within 15−20 min intervals representing the integral of the compositions encountered along flight segments of about 250 km. The overall uncertainty of the measured WAS CO is less than ±1% for the mixing ratio and ±0.1‰/±0.2‰ for $\delta^{13}C(CO)/\delta^{18}O(CO)$, respectively (Brenninkmeijer, 1993; Brenninkmeijer *et al.*, 2001). Isotope compositions are reported throughout this manuscript using the so-called delta value $\delta = (R/R_{st}-1)$ relating the ratio R of rare (^{13}C, ^{18}O or ^{17}O) over abundant isotopes of interest to the standard ratio R_{st}. These are V-SMOW of 2005.20×10^{-6} for $^{18}O/^{16}O$ (Gonfiantini, 1978; Coplen, 1994) and 386.72×10^{-6} for $^{17}O/^{16}O$ (Assonov and Brenninkmeijer, 2003), and V-PDB of 11237.2×10^{-6} for $^{13}C/^{12}C$ (Craig, 1957), respectively. As we mention above, the oxygen isotopic composition of the CO present in these WAS samples was corrupted, in particular when O_3 levels were as high as 100−600 nmol/mol.

[5] CARIBIC−2 (Phase #2, referred to as "C2") started operation in December 2004 with a Lufthansa *Airbus* A340-600 fitted with a new inlet system and air sampling lines, including PFA lined tubing for trace gas intake (Brenninkmeijer *et al.*, 2007). No flask CO mixing/isotope ratio measurements are performed in C2.

2.2 On-line instrumentation

[6] In addition to the WAS collection systems, both C1 and C2 measurement setups include different instrumentation for on-line detection of [CO] and [O_3] (hereinafter the squared brackets [] denote the abundance, *i.e.* concentration or mixing ratio, of the respective species). *In situ* CO analysis in C1 is done using a gas chromatography (GC)-reducing gas analyser which provides measurements every 130 s with uncertainty of ±3 nmol/mol (Zahn *et al.*, 2000). In C2, a vacuum ultraviolet fluorescence (VUV) instrument with lower measurement uncertainty and higher temporal resolution of ±2 nmol/mol in 2 s (Scharffe *et al.*, 2012) is employed, respectively. Furthermore, the detection frequency for O_3 abundances has also increased, *viz.*, from 0.06 Hz in C1 to 5 Hz in C2 (Zahn *et al.*, 2002; Zahn *et al.*, 2012).

2.3 Results

[7] When comparing the CO abundances in relation to those of O_3 for C1 and C2, differences are apparent in the LMS, where C2 CO values are systematically lower. This is illustrated in Fig. 1 (a) which presents the LMS CO-O_3 distribution of the C2 measurements overlaid with the C1 *in situ* and WAS data. (The entire C1 CO/O_3 dataset is presented in Fig. 2.) For the *in situ* CO datasets we calculated the statistics (Fig. 1 (b)) of the samples with respective O_3 abundances clustered in 20 nmol/mol bins, *i.e.* the median and spread of [CO] as a function of [O_3] analysed. (The interquartile range, IQR, is used in the current analysis as a robust measure of the data spread instead of the standard deviation.) The data exhibit large [CO] variations at [O_3] below 400 nmol/mol that primarily reflect pronounced seasonal variations in the NH tropospheric CO abundance. With O_3 rising, [CO] decreases to typical stratospheric values, and its spread reduces to mere 3.5 nmol/mol and less, as [O_3] surpasses 500 nmol/mol. Despite the comparable spread in C1 and C2 [CO], from 400 nmol/mol of [O_3] onwards the C1 CO mixing ratios start to level off, with no samples below 35 nmol/mol having been detected, whereas the C2 levels continuously decline. By the 580 nmol/mol O_3 bin, C1 [CO] of $39.7^{+0.7}_{-3}$ nmol/mol accommodates some extra 15 nmol/mol compared to $25.6^{+1.7}_{-1}$ nmol/mol typical for C2 values. Overall, at [O_3] above 400 nmol/mol the conspicuously high [CO] is marked in about 200 *in situ* C1 samples, of which 158 and 69 emerge as statistically significant mild and extreme outliers, respectively, when compared against the ample ($n > 3 \cdot 10^5$) C2 statistics. (The conventions here follow Natrella (2003), *i.e.* ±1.5 and ±3 IQR ranges define the inner and outer statistical fences (ranges outside which the data points are considered mild and extreme outliers) of the C2 [CO] distribution in every O_3 bin, respectively. The statistics include the samples in bins

with average [O_3] of 420−620 nmol/mol.) None of C1 CO at [O_3] above 560 nmol/mol agrees with the C2 observations. Because the CO levels cannot have changed over the period in question by the difference we find (up to 55%), artefacts and calibration issues need to be scrutinised.

[8] Unnatural elevations in the $^{18}O/^{16}O$ ratios of CO from WAS measurements are also evident, as shown in Figs. 3 and 4. The large $\delta^{18}O$(CO) departures that reach beyond +16‰ are found to be proportional to the concomitant O_3 abundances (denoted with colour) and more prominent at lower [CO]. A rather different relationship, however, is expected from our knowledge of UT/LMS CO sources (plus their isotope signatures) and available *in situ* observations (Fig. 2, shown with triangles), as elucidated by Brenninkmeijer *et al.* (1996) (hereafter denoted as "B96"). That is, the more stratospheric CO is, the greater fraction of its local inventory is refilled with the photochemical component stemming from methane oxidation with a characteristic $\delta^{18}O$ signature of ~0‰ or lower (Brenninkmeijer and Röckmann, 1997). This occurs because the CO sink at ruling UT/LMS temperatures proceeds more readily than its production, as the reaction of hydroxyl radical (OH) with CO, being primarily pressure-dependent, outcompetes the temperature-sensitive reaction of OH with CH_4. Furthermore, as the lifetime of CO quickly decreases with altitude, transport-mixing effects take the lead in determining the vertical distributions of [CO] and $\delta^{18}O$(CO) above the tropopause, hence their mutual relationship. This is seen from the B96 data at [CO] below 50 nmol/mol that line-up in a near linear relationship towards the end-members with lowest $^{18}O/^{16}O$ ratios. These result from the largest share of the ^{18}O-depleted photochemical component and extra depletion caused by the preferential removal of $C^{18}O$ in reaction with OH (fractionation about ~11‰ at pressures below 300 hPa, Stevens *et al.*, 1980; Röckmann *et al.*, 1998b).

[9] It is beyond doubt that the enhancements of C1 $C^{18}O$ originate from O_3, whose large enrichment in heavy oxygen (above +60‰ in $\delta^{18}O$, Brenninkmeijer *et al.*, 2003) is typical and found transferred to other atmospheric compounds (see Savarino and Morin (2012) for a review). In Fig. 2 it is also notable that not only the LMS compositions are affected but elevations of (3−10)‰ from the bulk $\delta^{18}O$(CO) values are present in more tropospheric samples with [CO] of up to ~100 nmol/mol. These result from the dilution of the least affected CO-rich tropospheric air by CO-poor, however substantially contaminated, stratospheric air, sampled into the same WAS tank. Such sampling-induced mixing renders an unambiguous determination of the artefact source' isotope signature rather difficult, because neither mixing nor isotope ratios of the admixed air portions are known sufficiently well (see below).

[10] Differences between the WAS and *in situ* measured [CO] – a possible indication that the $\delta^{18}O(CO)$ contamination pertains specifically to the WAS data – average at $\overline{\Delta}$(WAS−*in situ*) = (5.3±0.2) nmol/mol (±1 standard deviation of the mean, n = 408) and happen to be random with respect to any operational parameter or measured characteristic in C1, *i.e.* irrespective of CO or O_3 abundances. The above mentioned discrepancy remained after several calibrations between the two systems had been performed, and likely results from the differences in the detection methods, drifts of the calibration standards used (see details in Brenninkmeijer *et al.*, 2001) and a short-term production of CO in the stainless steel tanks during sampling. The large spread of Δ(WAS−*in situ*) of ±3.5 nmol/mol (±1σ of the population) ensues from the fact that the *in situ* sampled air corresponds to (2−4)% of the concomitantly sampled WAS volume, as typically 6−7 *in situ* collections of 5 s were made throughout one tank collection of 17−21 min. The integrity of the WAS CO is further affirmed by the unsystematic distribution of the artefact compositions among tanks (an opposite case for $\delta^{18}O(CO_2)$ in C1 is discussed by Assonov *et al.*, 2009). Overall, the WAS and *in situ* measured CO mixing ratios correlate extremely well (adj. R^2 = 0.972, slope of 0.992±0.008 (±1σ), n = 408). However, both anomalies in [CO] and $\delta^{18}O(CO)$ manifest clear but complex functions of the concomitant [O_3]. That is, the C1 *in situ* and WAS data very likely evidence artefacts pertaining to the O_3-driven effect of the same nature. Below we ascertain and quantify these.

3 Discussion

[11] Three factors may lead to the (artefact) distributions such as seen for C1 *in situ* [CO] at the LMS O_3 abundances, namely:

[12] (i) Strong (linear) natural mixing, such as enhanced stratosphere-troposphere exchange (STE), when a [CO] outside the statistically expected range results from the integration of air having dissimilar ratios of the tracers' abundances, *viz.* [O_3]:[CO]. For example, mixing of two air parcels in a 15%:85% proportion (by moles of air) with typical [O_3]:[CO] of 700:24 (stratospheric) and 60:125 (tropospheric), respectively, yields an integrated composition with [O_3]:[CO] of ~580:40 which indeed corresponds to C1 data (this case is exemplified by the mixing curve in Fig. 1). Nonetheless, occurrences of rather high (compared to the typical 24−26 nmol/mol) stratospheric CO mixing ratios (in our case, ~40 nmol/mol at the concomitant [O_3] of 500−600 nmol/mol) are rare. For instance, a deep STE similar to that described by Pan *et al.* (2004) was observed by C2 only once (*cf.* the outliers at [O_3] of 500 nmol/mol in Fig. 1), whereas the C1 outliers were exclusively registered in some 12 flights during

1997−2001. No relation between these outliers and the large-scale [CO] perturbation due to extensive biomass burning in 1997/1998 (Novelli *et al.*, 2003) is established, otherwise elevated CO mixing ratios should manifest themselves at lower [O_3] as well. Other tracers detected in CARIBIC provide supporting evidence against such strongly STE-mixed air having been captured by C1. That is, the binned distributions for the water vapour and de-trended N_2O (similar to that for [CO] *vs.* [O_3] presented in Fig. 1, not shown here) are greatly similar in C1 and C2. Whereas the small relative variations in atmospheric [N_2O] merely confirm matching [O_3] statistics in CARIBIC, the stratospheric [H_2O] distributions witness no [O_3]:[CO] values corresponding to those of the C1 outliers, suggesting the latter being unnaturally low.

[13] (ii) Mixing effects can also occur artificially, originating from sampling peculiarities or data processing. Since the CARIBIC platform is not stationary, about 5 s long sampling of an *in situ* air probe in C1 implies integration of the compositions encountered along some hundred metres, owing to the high aircraft speed. This distance may cover a transect between tropospheric and stratospheric filaments of much different compositions. The effect of such 'translational mixing' can be simulated by averaging the sampling data with higher temporal frequency over longer time intervals. In this respect, the substantially more frequent CO data in C2 (<1 s) were artificially averaged over a set of increasing intervals to reckon whether the long sampling period in C1 could be the culprit for skewing its CO−O_3 distribution. As a result, the original C2 data and their averages (equivalent to the C1 CO sample injection time) differ negligibly, as do the respective [O_3]:[CO] values. The actual C2 CO−O_3 statistic in the region of interest ([O_3] of 540−620 nmol/mol) remains insensitive to integration of up to 300 s. Furthermore, a very strong artificial mixing with an averaging interval of at least 1200 s (comparable to C1 WAS sampling time) is required to yield the averages from the C2 data with [O_3]:[CO] characteristic for the C1 outliers.

[14] (iii) In view of the above, it is unlikely that any natural or artificial mixing processes are involved in the stratospheric [CO] discrepancies seen in C1. We therefore conclude that the sample contamination in C1 occurred prior to the probed air reaching the analytical/sampling instrumentation in the container, since clearly elevated stratospheric CO mixing ratios are common to WAS and *in situ* data. Two more indications, *viz.* growing [CO] discrepancy with increasing O_3 abundance, and the strong concomitant signal in $\delta^{18}O(CO)$, imply that O_3-mediated photochemical production of CO took place. Further, by confronting the C1 and C2 [CO] measurements in a kinetic framework (detailed in Appendix A), we quantify the artefact CO component being chiefly a function of O_3 abundance as

$$C_c = b \cdot [O_3]^2,\ b = (5.19 \pm 0.12) \cdot 10^{-5}\ \text{[mol/nmol]}, \quad (1)$$

which is equivalent to 8−18 nmol/mol throughout the respective $[O_3]$ range of 400−620 nmol/mol (see Fig. 1 (d)). Subtracting this artefact signal yields the corrected *in situ* C1 CO−O_3 distribution conform to that of C2 (*cf.* red symbols in Fig. 1 (a)).

[15] Importantly, since we can quantify the contamination strength using only the O_3 abundance, the continuous *in situ* C1 $[O_3]$ data allows estimating the integral artefact CO component in each WAS sample and, if the isotope ratio of contaminating O_3 is known, to derive the initial $\delta^{18}O(CO)$. The latter, as it was mentioned above, is subject to strong sample-mixing effects, which is witnessed by $\delta^{18}O(CO)$ outliers even at relatively high [CO] up to 100 nmol/mol. Accounting for such cases is, however, problematic since it is necessary to distinguish the proportions of the least modified (tropospheric) and significantly affected (stratospheric) components in the resultant WAS sample mix. In reality, however, this information is not available, therefore we applied an *ad hoc* correction approach (which is capable of determining the contamination source (*i.e.*, O_3) isotope signature as well), as described in the following.

3.1 Contamination isotope signatures

[16] Practically we resort to the differential mixing model (MM, originally known as the "Keeling-plot"), because it requires only the estimate of the artefact component mixing ratio, but no assumptions on the (unknown) shares and isotope signatures of the air portions mixed in a given WAS tank. The MM parameterises the admixing of the portion of artefact CO to the WAS sample with the "true" initial composition, as formulated below:

$$\begin{cases} \delta_a C_a = C_t \delta_t + C_c \delta_c \\ C_a \equiv C_t + C_c \end{cases},$$

where indices *a*, *c* and *t* distinguish the abundances C and isotope compositions δ (^{13}C and ^{18}O) pertaining to the analysed sample, estimated contamination and "true" composition sought (*i.e.*, C_t and δ_t), respectively. (Here the contamination strength C_c is derived by integrating Eq. (1) using the *in situ* C1 $[O_3]$ data for each WAS sample.) By rewriting the above equation with respect to the isotope signature of the analysed CO, one obtains:

$$\delta_a = \delta_c + (\delta_t - \delta_c) C_t / C_a\ , \quad (2)$$

which signifies that linear regression of δ_a as a function of the reciprocal of C_a yields the estimated contamination signature δ_c at $(C_a)^{-1} \rightarrow 0$ when invariable "true" compositions (C_t, ${}^i\delta_t$) are taken (the Keeling plot detailing these calculations is shown in Fig. 5). We therefore apply the

MM described by Eq. (2) to the subsets of samples picked according to the same reckoned C_t (within a ±2 nmol/mol window, $n > 7$). Such selection, however, may be insufficient: Due to the strong sampling effects in the WAS samples (see previous Section), it is possible to encounter samples that integrate different air masses to the same C_t but rather different average δ_t. The solution in this case is to refer to the goodness of the MM regression fit, because the R^2 intrinsically measures the linearity of the regressed data, *i.e.* closeness of the "true" values in a regarded subset of samples, irrespective of underlying reasons for that.

[17] Higher R^2 values thus imply higher consistency of the estimate, as demonstrated in Fig. 6 showing the calculated δ_c for C_t below 80 nmol/mol as a function of the regression R^2. The latter decreases with greater C_t (*i.e.*, larger sample subset size, since tropospheric air is more often encountered) and, conformably, larger variations in δ_t. Ultimately, at lower R^2 the inferred ^{18}O signatures converge to values slightly above zero expected for uncorrelated data, *i.e.* C1 $\delta^{18}O(CO)$ tropospheric average. A similar relationship is seen for the ^{13}C signatures (they converge around −28‰), however, there are no consistent estimates found (R^2 is generally below 0.4). Since such is not the case for $\delta^{18}O$, the MM is not sufficiently sensitive to the changes caused by the contamination, which implies that the artefact CO $\delta^{13}C$ should be within the range of the "true" $\delta^{13}C(CO)$ values. Interestingly, the MM is rather responsive to the growing fraction of the CH_4-derived component in CO with increasing $[O_3]$, as the $^{13}\delta_c$ value of −(47.2±5.8)‰ inferred at R^2 above 0.4 is characteristic for the $\delta^{13}C$ of methane in the UT/LMS. It is important to note that we have accounted for the biases in the analysed C1 WAS $\delta^{13}C(CO)$ expected from the mass-independent isotope composition of O_3 (see details in Appendix B).

[18] We derive the "best-guess" estimate of the admixed CO ^{18}O signature at $^{18}\delta_c$ = +(92.0±8.3)‰, which agrees with the other MM results obtained at R^2 above 0.75. Taking the same subsets of samples, the concomitant ^{13}C signature matches $^{13}\delta_c$ = −(23.3±8.6)‰, indeed at the upper end of the expected LMS $\delta^{13}C(CO)$ variations of −(25−31)‰. Because of that, the MM is likely insensitive to the changes in $\delta^{13}C(CO)$ caused by the contamination (the corresponding R^2 values are below 0.1). Upon the correction using the inferred $^{18}\delta_c$ value, the C1 WAS $\delta^{18}O(CO)$ data appear adequate (shown with red symbols in Fig. 2). That is, variations in the observed $C^{18}O$ are driven by (i) the seasonal/regional changes in the composition of tropospheric air and by (ii) the degree of mixing or replacement of the latter with the stratospheric component that is less variable in ^{18}O. This is seen as stretching of the scattered tropospheric values ([CO] above 60 nmol/mol) in a mixing fashion towards $\delta^{18}O(CO)$ of around −10‰ at [CO] of ~25 nmol/mol, respectively. The corrected C1 $\delta^{13}C(CO)$ data (shown in Fig. 7) are

found to be in a ±1‰ agreement with the observations by B96, except for several deep stratospheric samples ([CO] below 40 nmol/mol). The latter were encountered during "ozone hole" conditions and carried extremely low ^{13}CO abundances, which was attributed to the reaction of methane with available free Cl radicals (Brenninkmeijer *et al.*, 1996).

3.2 Estimate of $\delta^{18}O(O_3)$

[19] The contamination ^{18}O signature inferred here ($^{18}\delta_c$ = +(92.0±8.3)‰) unambiguously pertains to O_3 and is comparable to $\delta^{18}O(O_3)$ values measured in the stratosphere at temperatures about 30 K lower than those encountered in the UT/LMS by C1 (see Table 1 for comparison). If no other factors are involved (see below), this discrepancy in $\delta^{18}O(O_3)$ should be attributed to the local conditions, *i.e.* the higher pressures (typically 240−270 hPa for C1 cruising altitudes) at which O_3 was formed. Indeed, the molecular lifetime (the period through which the species' isotope reservoir becomes entirely renewed, as opposed to the "bulk" lifetime) of O_3 encountered along the C1 flight routes is estimated on the order of minutes to hours at daylight (H. Riede, Max Planck Institute for Chemistry, 2010), thus the isotope composition of the photochemically regenerated O_3 resets quickly according to the local conditions. Virtual absence of sinks, in turn, leads to "freezing" of the $\delta^{18}O(O_3)$ value during night in the UT/LMS. Verifying the current $\delta^{18}O(O_3)$ estimate against the kinetic data, in contrast to the stratospheric cases, is problematic. The laboratory studies on O_3 formation to date have scrutinised the concomitant kinetic isotope effects (KIEs) as a function of temperature at only low pressures (50 Torr); the attenuation of the KIEs with increasing pressure was studied only at room temperatures (see Table 1, also Brenninkmeijer *et al.* (2003) for references). A rather crude attempt may be undertaken by assuming that the formation KIEs become attenuated at higher pressures in a similar (proportional) fashion to that measured at 320 K, however applied to the nominal low-pressure values reckoned at (220−230) K. A decrease in $\delta^{18}O(O_3)$ of about (5.9−7.6)‰ is expected from such calculation, yet accounting for a mere one-half of the (13.3−14.6)‰ discrepancy between the stratospheric $\delta^{18}O(O_3)$ values and $^{18}\delta_c$.

[20] Lower $^{18}\delta_c$ values could result from possible isotope fractionation accompanying the production of the artefact CO. Although not quantifiable here, oxygen KIEs in the $O_3 \rightarrow CO$ conversion chain cannot be ruled out, recalling that the intermediate reaction steps are not identifiable and the artefact CO represents at most 4% of all O_3 molecules. Furthermore, the yield λ_{O_3} of CO from O_3 may be lower than unity (see details in Appendix A). On the other hand, the inference that the contamination strength primarily depends on $[O_3]$ indicates that the kinetic frac-

tionation may have greater effect on the carbon isotope ratios of the artefact CO produced (the $^{13}\delta_c$ values) in contrast to the oxygen ones. That is because all reactive oxygen available from O_3 becomes converted to CO, whilst the concomitant carbon atoms are drawn from a virtually unlimited pool whose apparent isotope composition is altered by the magnitude of the ^{13}C KIEs.

[21] Besides KIEs, selectivity in the transfer of O atoms from O_3 to CO affects the resulting $^{18}\delta_c$ value. The terminal O atoms in O_3 are enriched with respect to the molecular (bulk) O_3 composition when the latter is above ~+70‰ in $\delta^{18}O$ (Janssen, 2005; Bhattacharya *et al.*, 2008), therefore an incorporation of only central O atoms into the artefact CO molecules should result in a reduced apparent $^{18}\delta_c$ value. Such exclusive selection is, however, less likely from the kinetic standpoint and was not observed in available laboratory studies (see Savarino *et al.* (2008) for a review). For instance, Röckmann *et al.* (1998a) established the evidence of direct O transfer from O_3 to the CO produced in alkene ozonolysis. A reanalysis of their results (in light of findings of Bhattacharya *et al.* (2008)) suggests that usually the terminal atoms of the O_3 molecule become transferred (their ratio over the central ones changes from the bulk ~2:1 to ~1:0 for various species). Considering the alternatives of the O transfer in our case (listed additionally in Table 1), the equiprobable incorporation of the terminal and central O_3 atoms into CO should result in the $\delta^{18}O(O_3)$ value in agreement with the "crude" estimate based on laboratory data given above.

[22] Furthermore, the conditions that supported the reaction of O_3 (or its derivatives) followed by the production of CO are vague. A few hypotheses ought to be scrutinised here. First, a fast $O_3 \rightarrow$ CO conversion must have occurred, owing to short (*i.e.*, fraction of a second) exposure time of the probed air to the contamination. Accounting for the typical C1 air sampling conditions (these are: sampled air pressure of 240−270 hPa and temperature of 220−235 K outboard to 275−300 K inboard, sampling rate of ~$12.85 \cdot 10^{-3}$ moles s^{-1} corresponding to 350 L STP sampled in 1200 s, inlet/tubing volume gauged to yield exposure times of 0.01 to 0.1 s due to variable air intake rate, $[O_3]$ of 600 nmol/mol), the overall reaction rate coefficient (k_c in Eq. (A1) from Appendix A) must be on the order of $(6 \cdot 10^{-15}/\tau_c)$ $molec^{-1}$ cm^3 s^{-1}, where τ_c is the exposure time. Assuming the case of a gas-phase CO production from a recombining O_3 derivative and an unknown carbonaceous compound X, the reaction rate coefficient for the latter ($^X k_r$ in Eq. (A1) in Appendix A) must be unrealistically high, at least ~$6 \cdot 10^{-10}$ $molec^{-1}$ cm^3 s^{-1} over τ_c = 1/100 s. This number decreases proportionally with growing τ_c and [X], if we take less strict exposure conditions. Nonetheless, in order to provide the amounts of artefact CO we detect, a

minimum abundance of 20 nmol/mol (or up to 4 μg of C per flight) of X is required, which is not available in the UT/LMS from the species readily undergoing ozonolysis, *e.g.* alkenes.

[23] Second, a more complex heterogeneous chemistry on the inner surface of the inlet or supplying tubing may be involved. Such can be the tracers' surface adsorption, (catalytic) decomposition of O_3 and its reaction with organics or with surface carbon that also may lead to the production of CO (Oyama, 2000). Evidence exists for the dissociative adsorption of O_3 on the surfaces with subsequent production of the reactive atomic oxygen species (see, *e.g.*, Li *et al.*, 1998, also Oyama, 2000). It is probable that sufficient amounts of organics have remained on the walls of the sampling line exposed to highly polluted tropospheric air, to be later broken down by the products of the heterogeneous decomposition of the ample stratospheric O_3. Unfortunately, the scope for a detailed quantification of intricate surface effects in the C1 CO contamination problem is very limited.

4 Conclusions

[24] Recapitulating, the *in situ* measurements of CO and O_3 allowed us to unambiguously quantify the artefact CO production from O_3 likely in the sample line of the CARIBIC−1 instrumentation. Strong evidence to that is provided by the isotope CO measurements. We demonstrate the ability of the simple mixing model ("Keeling-plot" approach) to single out the contamination isotope signatures even in the case of a large sampling-induced mixing of the air with very different compositions. Obtained as a collateral result, the estimate of the $\delta^{18}O(O_3)$ in the UT/LMS appears adequate, calling, however, for additional laboratory data (*e.g.*, the temperature-driven variations of the O_3 formation KIE at pressures above 100 hPa) for a more unambiguous verification.

Appendix A. Contamination kinetic framework

[25] We infer the functional dependence of the CO contamination strength in the kinetic framework conceptually formulated as follows:

$$\mathrm{O_3} \xrightarrow{{}^{\mathrm{O_3}}k_1} \left(\begin{array}{l} \left(\ldots + \mathrm{X} \xrightarrow{{}^{\mathrm{X}}k_r} \ldots \right)_K \\ \left(\ldots + \mathrm{O_3} \xrightarrow{{}^{\mathrm{O_3}}k_r} \ldots \right)_{(\kappa-1)} \end{array} \right) \rightarrow \lambda_{\mathrm{O_3}} \mathrm{CO} \ . \qquad \text{(A1)}$$

Eq. (A1) reads that production of an artefact CO molecules is initiated by O_3 (via either its decomposition or a reaction with an unknown educt) and is followed by a set of unknown reac-

tions which proceed via unknown educts or products (denoted with ellipses), however requiring at some step an incorporation of carbon (donated by carbonaceous species X) and oxygen (also possible in secondary O_3 reactions) atoms into final CO. Coefficients K and κ describe the stoichiometry of the system, *i.e.* how many reactions of X and O_3 (with the individual unknown rate coefficients ${}^{X}k_r$ and ${}^{O_3}k_r$) lead to production of one artefact CO, respectively. The yield λ_{O_3}, a diagnostic quantity, relates the amount of artefact CO molecules produced to the total number of O_3 molecules consumed in the system. Based on Eq. (A1), the functional dependence of the artefact CO component (denoted C_c, obtained by discriminating the C1 outliers from respective C2 data) on $[O_3]$ or [X] is generally formulated as (abundances in number density units are used)

$$C_c = \int_{\tau_c} \prod_{\kappa} {}^{O_3}k_r [O_3] \prod_{K} {}^{X}k_r [X] dt \ , \tag{A2}$$

where τ_c denotes the contamination reaction time. Eq. (A2) defines the regression expression using which we attempted to fit the values of C_c as a function of κ, $[O_3]$, K and [X] (the latter was chosen iteratively from a set of carbonaceous species measured). Practically, however, this regression analysis ascertains that variations in C_c are exhaustively described using $[O_3]$ and κ. Furthermore, we find that no other species or operational parameter (*e.g.* temperature, pressure, flight duration, latitude, *etc.*) measured in C1 appear to determine (correlate with) C_c. Based on this, we can reduce Eq. (A2) to its final, simpler form, *viz.*

$$C_c = \lambda_{O_3} k_c [O_3]^{\kappa} \tau_c \ , \tag{A3}$$

where k_c denotes the overall pseudo-first-order rate coefficient of the reaction chain that is exclusively propelled by O_3. The product $(\lambda_{O_3} k_c \tau_c)$ thus integrates the influence of the unknown (and likely invariable) [X], ${}^{X}k_r$, K and τ_c. Finally, regressing C_c using Eq. (A3) provides its best approximation as a function of $[O_3]$ at $\kappa = 2.06 \pm 0.38$, suggesting two chain steps involving O_3 or its derivatives. At $\kappa = 2$, the product $(\lambda_{O_3} k_c \tau_c)$ that proportionates the CO contamination strength and $[O_3]$ is found to be $(5.19 \pm 0.12) \cdot 10^{-5}$ mol/nmol ($\pm 1\sigma$, adj. $R^2 = 0.83$, red. $\chi^2 = 4.0$; mole fraction units are used here for convenience). The low uncertainty (within ±3%) of this estimate confirms an exclusive dependence of the contamination source on the O_3 abundance, as well as much similar reaction times τ_c. The regressed value of C_c as a function of $[O_3]$ is presented in Fig. 1 (d) (solid line). It is possible to constrain the overall yield λ_{O_3} of CO molecules in the artefact source chain to be between 0.5 and 1, comparing the magnitude of C_c to the discrepancy between the $[O_3]$ measured in C1 and C2 (±20 nmol/mol, taken equal to the $[O_3]$ bin

size owing to the $N_2O{-}O_3$ and $H_2O{-}O_3$ distributions matching well between the datasets). Lower λ_{O_3} values, otherwise, should have resulted in a noticeable (*i.e.*, greater than 20 nmol/mol) decrease in the C1 O_3 abundances with respect to the C2 levels.

Appendix B. Corrections to measured $\delta^{13}C(CO)$ values due to the oxygen MIF

[26] Atmospheric O_3 carries an anomalous isotope composition (or mass-independent fractionation, MIF) with a substantially higher relative enrichment in ^{17}O over that in ^{18}O (above +25‰ in $\Delta^{17}O = (\delta^{17}O+1)/(\delta^{18}O+1)^{\beta}-1$, $\beta = 0.528$) when compared to the majority of terrestrial oxygen reservoirs that are mass-dependently fractionated (*i.e.*, with $\Delta^{17}O$ of ~0‰) (see Brenninkmeijer *et al.* (2003) and refs. therein). CO itself also has an unusual oxygen isotopic composition, possessing a moderate tropospheric MIF of around +5‰ in $\Delta^{17}O(CO)$ induced by the sink KIEs in reaction of CO with OH (Röckmann *et al.*, 1998b; Röckmann *et al.*, 2002) and a minor source effect from the ozonolysis of alkenes (Röckmann *et al.*, 1998a; Gromov *et al.*, 2010). A substantial contamination of CO by O_3 oxygen induces proportional changes to $\Delta^{17}O(CO)$ that largely exceed its natural atmospheric variation. On the other hand, the MIF has implications in the analytical determination of $\delta^{13}C(CO)$, because the presence of $C^{17}O$ species interferes with the mass-spectrometric measurement of the abundances of ^{13}CO possessing the same basic molecular mass (*m/z* is 45). When inferring the exact $C^{17}O/C^{18}O$ ratio in the analysed sample is not possible, analytical techniques usually involve assumptions (*e.g.*, mass-dependently fractionated compositions or a certain non-zero $\Delta^{17}O$ value) with respect to the $C^{17}O$ abundances (Assonov and Brenninkmeijer, 2001). In effect for the C1 CO data, the artefact CO produced from O_3 had contributed with unexpectedly high $C^{17}O$ abundances that led to the overestimated $\delta^{13}C(CO)$ analysed. The respective bias ${}^{13}\delta_b$ is quantified using

$$ {}^{13}\delta_b = 7.26\cdot10^{-2}\,\Delta^{17}O(CO)\,, \qquad \text{(B1)} $$

where the actual $\Delta^{17}O(CO)$ value is approximated from the natural CO MIF signal ${}^{17}\Delta_n$ and the typical O_3 MIF composition ${}^{17}\Delta_c$ as

$$ \Delta^{17}O(CO) = ({}^{17}\Delta_n\,(C_a - C_c) + {}^{17}\Delta_c\,C_c)(C_a)^{-1}\,. \qquad \text{(B2)} $$

Here C_a and C_c denote the analysed CO abundance and contamination magnitude, respectively, used in the contamination kinetic framework (see Appendix A, Eq. (A3)) and in calculations with the MM (see Sect. 3.1) . For the purpose of the current estimate it is sufficient to take ${}^{17}\Delta_n$ of +5‰ representing equilibrium enrichments expected in the remote free troposphere and UT/

LMS. For the O_3 MIF signature $^{17}\Delta_c$, the value of +30‰ (the average $\Delta^{17}O(O_3)$ expected from the kinetic laboratory data at conditions met along the C1 flight routes, see Sect. 3.2 and Table 1) is adopted. The coefficient that proportionates $^{13}\delta_b$ and $\Delta^{17}O$ in Eq. (B1) is derived by linearly regressing the $\delta^{13}C(CO)$ biases (simulated using the calculation apparatus detailed by Assonov and Brenninkmeijer, 2001) as a function of $\Delta^{17}O(CO)$ varying within a (0−30)‰ range for the CO with initially unaccounted MIF (*e.g.*, the sample is assumed to be mass-dependently fractionated). It therefore quantifies some extra +(0.726±0.003)‰ in the analysed $\delta^{13}C(CO)$ per every +10‰ of $\Delta^{17}O(CO)$ excess. The most contaminated C1 WAS CO samples at $[O_3]$ above 300 nmol/mol are estimated to bear $\Delta^{17}O(CO)$ of (6−12)‰ corresponding to fractions of (0.10−0.27) of the artefact CO in the sample. Accordingly, the reckoned $\delta^{13}C(CO)$ biases span (0.5−0.9)‰. Although not large, these well exceed the $\delta^{13}C(CO)$ measurement precision of ±0.1‰ and were corrected for, and therefore are taken into account in the calculations with the MM presented in Sect. 3.1.

Acknowledgements

[27] The authors are indebted to Claus Koeppel, Dieter Scharffe and Dr. Andreas Zahn for their work and expertise on the carbon monoxide and ozone measurements in C1 and C2. Hella Riede is acknowledged for comprehensive estimates of the species lifetimes along the CARIBIC flight routes. We are grateful to Dr. Taku Umezawa, Dr. Angela K. Baker, Dr. Emma C. Leedham, Dr. Sergey Assonov, the anonymous reviewer and Dr. Jan Kaiser for the helpful discussions and comments on the manuscript.

References

Assonov, S. S. and Brenninkmeijer, C. A. M.: A new method to determine the ^{17}O isotopic abundance in CO_2 using oxygen isotope exchange with a solid oxide, *Rapid Commun. Mass Spectrom.*, **15**, 2426−2437, doi: 10.1002/rcm.529, 2001.

Assonov, S. S. and Brenninkmeijer, C. A. M.: A redetermination of absolute values for $^{17}R_{VPDB\text{-}CO2}$ and $^{17}R_{VSMOW}$, *Rapid Commun. Mass Spectrom.*, **17**, 1017−1029, doi: 10.1002/Rcm.1011, 2003.

Assonov, S. S., Brenninkmeijer, C. A. M., Koeppel, C., and Röckmann, T.: CO_2 isotope analyses using large air samples collected on intercontinental flights by the CARIBIC Boeing 767, *Rapid Commun. Mass Spectrom.*, **23**, 822−830, doi: 10.1002/rcm.3946, 2009.

Bhattacharya, S. K., Pandey, A., and Savarino, J.: Determination of intramolecular isotope distribution of ozone by oxidation reaction with silver metal, *J. Geophys. Res. Atm.*, **113**, D03303, doi: 10.1029/2006jd008309, 2008.

Brenninkmeijer, C. A. M.: Measurement of the abundance of ^{14}CO in the atmosphere and the $^{13}C/^{12}C$ and $^{18}O/^{16}O$ ratio of atmospheric CO with applications in New Zealand and Antarctica, *J. Geophys. Res. Atm.*, **98**, 10595−10614, doi: 10.1029/93JD00587, 1993.

Brenninkmeijer, C. A. M., Müller, R., Crutzen, P. J., Lowe, D. C., Manning, M. R., Sparks, R. J., and van Velthoven, P. F. J.: A large ^{13}CO deficit in the lower Antarctic stratosphere due to "Ozone Hole" Chemistry: Part I, Observations, *Geophys. Res. Lett.*, **23**, 2125−2128, doi: 10.1029/96gl01471, 1996.

Brenninkmeijer, C. A. M. and Röckmann, T.: Principal factors determining the $^{18}O/^{16}O$ ratio of atmospheric CO as derived from observations in the southern hemispheric troposphere and lowermost stratosphere, *J. Geophys. Res. Atm.*, **102**, 25477−25485, doi: 10.1029/97JD02291, 1997.

Brenninkmeijer, C. A. M., Crutzen, P. J., Fischer, H., Gusten, H., Hans, W., Heinrich, G., Heintzenberg, J., Hermann, M., Immelmann, T., Kersting, D., Maiss, M., Nolle, M., Pitscheider, A., Pohlkamp, H., Scharffe, D., Specht, K., and Wiedensohler, A.: CARIBIC – Civil aircraft for global measurement of trace gases and aerosols in the tropopause region, *J. Atmos. Oceanic Technol.*, **16**, 1373−1383, doi: 10.1175/1520-0426(1999)016<1373:Ccafgm>2.0.Co;2, 1999.

Brenninkmeijer, C. A. M., Koeppel, C., Röckmann, T., Scharffe, D. S., Bräunlich, M., and Gros, V.: Absolute measurement of the abundance of atmospheric carbon monoxide, *J. Geophys. Res. Atm.*, **106**, 10003−10010, doi: 10.1029/2000jd900342, 2001.

Brenninkmeijer, C. A. M., Janssen, C., Kaiser, J., Röckmann, T., Rhee, T. S., and Assonov, S. S.: Isotope effects in the chemistry of atmospheric trace compounds, *Chem. Rev.*, **103**, 5125−5161, doi: 10.1021/Cr020644k, 2003.

Brenninkmeijer, C. A. M., Crutzen, P., Boumard, F., Dauer, T., Dix, B., Ebinghaus, R., Filippi, D., Fischer, H., Franke, H., Frieβ, U., Heintzenberg, J., Helleis, F., Hermann, M., Kock, H. H., Koeppel, C., Lelieveld, J., Leuenberger, M., Martinsson, B. G., Miemczyk, S., Moret, H. P., Nguyen, H. N., Nyfeler, P., Oram, D., O'Sullivan, D., Penkett, S., Platt, U., Pupek, M., Ramonet, M., Randa, B., Reichelt, M., Rhee, T. S., Rohwer, J., Rosenfeld, K., Scharffe, D., Schlager, H., Schumann, U., Slemr, F., Sprung, D., Stock, P., Thaler, R., Valentino, F., van Velthoven, P., Waibel, A., Wandel, A., Waschitschek, K., Wiedensohler, A., Xueref-Remy, I., Zahn, A., Zech, U., and Ziereis, H.: Civil Aircraft for the regular investigation of the atmosphere based on an instrumented container: The new CARIBIC system, *Atmos. Chem. Phys.*, **7**, 4953−4976, doi: 10.5194/acp-7-4953-2007, 2007.

Coplen, T. B.: Reporting of stable hydrogen, carbon, and oxygen isotopic abundances (Technical Report), *Pure Appl. Chem.*, **66**, 273−276, doi: 10.1351/pac199466020273, 1994.

Craig, H.: Isotopic standards for carbon and oxygen and correction factors for mass-spectrometric analysis of carbon dioxide, *Geochim. Cosmochim. Acta*, **12**, 133−149, doi: 10.1016/0016-7037(57)90024-8, 1957.

Gonfiantini, R.: Standards for Stable Isotope Measurements in Natural Compounds, *Nature*, **271**, 534−536, 1978.

Gromov, S., Jöckel, P., Sander, R., and Brenninkmeijer, C. A. M.: A kinetic chemistry tagging technique and its application to modelling the stable isotopic composition of atmospheric trace gases, *Geosci. Model Dev.*, **3**, 337−364, doi: 10.5194/gmd-3-337-2010, 2010.

Guenther, J., Erbacher, B., Krankowsky, D., and Mauersberger, K.: Pressure dependence of two relative ozone formation rate coefficients, *Chem. Phys. Lett.*, **306**, 209−213, doi: 10.1016/S0009-2614(99)00469-8, 1999.

Janssen, C., Guenther, J., Krankowsky, D., and Mauersberger, K.: Temperature dependence of ozone rate coefficients and isotopologue fractionation in $^{16}O-^{18}O$ oxygen mixtures, *Chem. Phys. Lett.*, **367**, 34−38, doi: 10.1016/S0009-2614(02)01665-2, 2003.

Janssen, C.: Intramolecular isotope distribution in heavy ozone ($^{16}O^{18}O^{16}O$ and $^{16}O^{16}O^{18}O$), *J. Geophys. Res. Atm.*, **110**, D08308, doi: 10.1029/2004jd005479, 2005.

Johnston, J. C. and Thiemens, M. H.: The isotopic composition of tropospheric ozone in three environments, *J. Geophys. Res. Atm.*, **102**, 25395−25404, doi: 10.1029/97jd02075, 1997.

Krankowsky, D., Bartecki, F., Klees, G. G., Mauersberger, K., Schellenbach, K., and Stehr, J.: Measurement of heavy isotope enrichment in tropospheric ozone, *Geophys. Res. Lett.*, **22**, 1713−1716, doi: 10.1029/95gl01436, 1995.

Krankowsky, D., Lämmerzahl, P., Mauersberger, K., Janssen, C., Tuzson, B., and Röckmann, T.: Stratospheric ozone isotope fractionations derived from collected samples, *J. Geophys. Res. Atm.*, **112**, D08301, doi: 10.1029/2006jd007855, 2007.

Li, W., Gibbs, G. V., and Oyama, S. T.: Mechanism of Ozone Decomposition on a Manganese Oxide Catalyst. 1. In Situ Raman Spectroscopy and Ab Initio Molecular Orbital Calculations, *J. Am. Chem. Soc.*, **120**, 9041−9046, doi: 10.1021/ja981441+, 1998.

Mauersberger, K.: Measurement of Heavy Ozone in the Stratosphere, *Geophys. Res. Lett.*, **8**, 935−937, doi: 10.1029/Gl008i008p00935, 1981.

Natrella, M.: NIST/SEMATECH e-Handbook of Statistical Methodsed., edited by: Croarkin, C. and Tobias, P., NIST/SEMATECH, http://www.itl.nist.gov/div898/handbook/ (last access: 07 May 2014), 2003.

Novelli, P. C., Masarie, K. A., and Lang, P. M.: Distributions and recent changes of carbon monoxide in the lower troposphere, *J. Geophys. Res.*, **103**, 19015−19033, doi: 10.1029/98jd01366, 1998.

Novelli, P. C., Masarie, K. A., Lang, P. M., Hall, B. D., Myers, R. C., and Elkins, J. W.: Reanalysis of tropospheric CO trends: Effects of the 1997−1998 wildfires, *J. Geophys. Res.*, **108**, 4464, doi: 10.1029/2002jd003031, 2003.

Oyama, S. T.: Chemical and Catalytic Properties of Ozone, *Catal. Rev. Sci. Eng.*, **42**, 279−322, doi: 10.1081/cr-100100263, 2000.

Pan, L. L., Randel, W. J., Gary, B. L., Mahoney, M. J., and Hintsa, E. J.: Definitions and sharpness of the extratropical tropopause: A trace gas perspective, *J. Geophys. Res. Atm.*, **109**, D23103, doi: 10.1029/2004jd004982, 2004.

Röckmann, T., Brenninkmeijer, C. A. M., Neeb, P., and Crutzen, P. J.: Ozonolysis of nonmethane hydrocarbons as a source of the observed mass independent oxygen isotope enrichment in tropospheric CO, *J. Geophys. Res. Atm.*, **103**, 1463−1470, doi: 10.1029/97JD02929, 1998a.

Röckmann, T., Brenninkmeijer, C. A. M., Saueressig, G., Bergamaschi, P., Crowley, J. N., Fischer, H., and Crutzen, P. J.: Mass-independent oxygen isotope fractionation in atmospheric CO as a result of the reaction CO+OH, *Science*, **281**, 544−546, doi: 10.1126/science.281.5376.544, 1998b.

Röckmann, T., Jöckel, P., Gros, V., Bräunlich, M., Possnert, G., and Brenninkmeijer, C. A. M.: Using ^{14}C, ^{13}C, ^{18}O and ^{17}O isotopic variations to provide insights into the high northern latitude surface CO inventory, *Atmos. Chem. Phys.*, **2**, 147−159, doi: 10.5194/acp-2-147-2002, 2002.

Savarino, J., Bhattacharya, S. K., Morin, S., Baroni, M., and Doussin, J. F.: The $NO+O_3$ reaction: A triple oxygen isotope perspective on the reaction dynamics and atmospheric implications for the transfer of the ozone isotope anomaly, *J. Chem. Phys.*, **128**, 194303, doi: 10.1063/1.2917581, 2008.

Savarino, J. and Morin, S.: The N, O, S Isotopes of Oxy-Anions in Ice Cores and Polar Environments, in: Handbook of Environmental Isotope Geochemistry, edited by: Baskaran, M., Advances in Isotope Geochemistry, Springer Berlin Heidelberg, 835−864, 2012.

Scharffe, D., Slemr, F., Brenninkmeijer, C. A. M., and Zahn, A.: Carbon monoxide measurements onboard the CARIBIC passenger aircraft using UV resonance fluorescence, *Atmos. Meas. Tech.*, **5**, 1753−1760, doi: 10.5194/amt-5-1753-2012, 2012.

Schinke, R., Grebenshchikov, S. Y., Ivanov, M. V., and Fleurat-Lessard, P.: Dynamical Studies Of The Ozone Isotope Effect: A Status Report, *Annu. Rev. Phys. Chem.*, **57**, 625−661, doi: 10.1146/annurev.physchem.57.032905.104542, 2006.

Stevens, C. M., Kaplan, L., Gorse, R., Durkee, S., Compton, M., Cohen, S., and Bielling, K.: The Kinetic Isotope Effect for Carbon and Oxygen in the Reaction CO+OH, *Int. J. Chem. Kinet.*, **12**, 935−948, doi: 10.1002/kin.550121205, 1980.

Vicars, W. C., Bhattacharya, S. K., Erbland, J., and Savarino, J.: Measurement of the ^{17}O-excess (Δ^{17}O) of tropospheric ozone using a nitrite-coated filter, *Rapid Commun. Mass Spectrom.*, **26**, 1219−1231, doi: 10.1002/rcm.6218, 2012.

Vicars, W. C. and Savarino, J.: Quantitative constraints on the ^{17}O-excess (Δ^{17}O) signature of surface ozone: Ambient measurements from 50°N to 50°S using the nitrite-coated filter technique, *Geochim. Cosmochim. Acta*, **135**, 270−287, doi: 10.1016/j.gca.2014.03.023, 2014.

Zahn, A., Brenninkmeijer, C. A. M., Maiss, M., Scharffe, D. H., Crutzen, P. J., Hermann, M., Heintzenberg, J., Wiedensohler, A., Güsten, H., Heinrich, G., Fischer, H., Cuijpers, J. W. M., and van Velthoven, P. F. J.: Identification of extratropical two-way troposphere-stratosphere mixing based on CARIBIC measurements of O_3, CO, and ultrafine particles, *J. Geophys. Res.*, **105**, 1527−1535, doi: 10.1029/1999jd900759, 2000.

Zahn, A., Brenninkmeijer, C. A. M., Asman, W. A. H., Crutzen, P. J., Heinrich, G., Fischer, H., Cuijpers, J. W. M., and van Velthoven, P. F. J.: Budgets of O_3 and CO in the upper troposphere: CARIBIC passenger aircraft results 1997–2001, *J. Geophys. Res. Atm.*, **107**, 4337, doi: 10.1029/2001jd001529, 2002.

Zahn, A., Weppner, J., Widmann, H., Schlote-Holubek, K., Burger, B., Kühner, T., and Franke, H.: A fast and precise chemiluminescence ozone detector for eddy flux and airborne application, *Atmos. Meas. Tech.*, **5**, 363−375, doi: 10.5194/amt-5-363-2012, 2012.

Tables

Table 1. Ozone $^{18}O/^{16}O$ isotope ratios from literature and this study

Domain	T (K)	P (hPa)	$\delta^{18}O(O_3)$ (‰)	Remarks
Stratosphere	190−210	13−50	83−93 (<3)	[1]
UT/LMS	220−235	240−270	89−95 (8)	[2]
			84−88 (6)	T
			91−98 (9)	TC
			112−124 (17)	C
Laboratory	190−210	~67	87−97 (6)	[3]
	220−235	~67	102−110 (6)	[3]
	220−235	240−270	95−103	[4]

Notes: Values in parentheses denote the average of the estimates' standard errors. The expected O_3 isotope composition on the V-SMOW scale is calculated from the O_3 enrichments ε reported relative to O_2 using $\delta^{18}O(O_3)_{V\text{-}SMOW} = \delta^{18}O(O_2)_{V\text{-}SMOW} + {}^{18}\varepsilon(O_3)_{O_2} + [\delta^{18}O(O_2)_{V\text{-}SMOW} \times {}^{18}\varepsilon(O_3)_{O_2}]$.

[1] Observations (see Krankowsky *et al.* (2007) and refs. therein), lowermost values (19−25 km). Quoted temperature range is derived by matching measured $\delta^{18}O(O_3)$ and laboratory data (see note [3]).

[2] This study, C1 observations (10−12 km). Letters denote the estimates derived using the data from Bhattacharya *et al.* (2008) and assuming only terminal (T), only central (C) and equiprobable terminal and central (TC) O_3 atoms transfer to the artefact CO.

[3] Calculated using the laboratory KIE temperature dependence data summarised by Janssen *et al.* (2003).

[4] Calculated assuming a pressure dependence of the O_3 formation KIE similar to that measured at 320 K (see Guenther *et al.* (1999) and refs. therein).

Figures

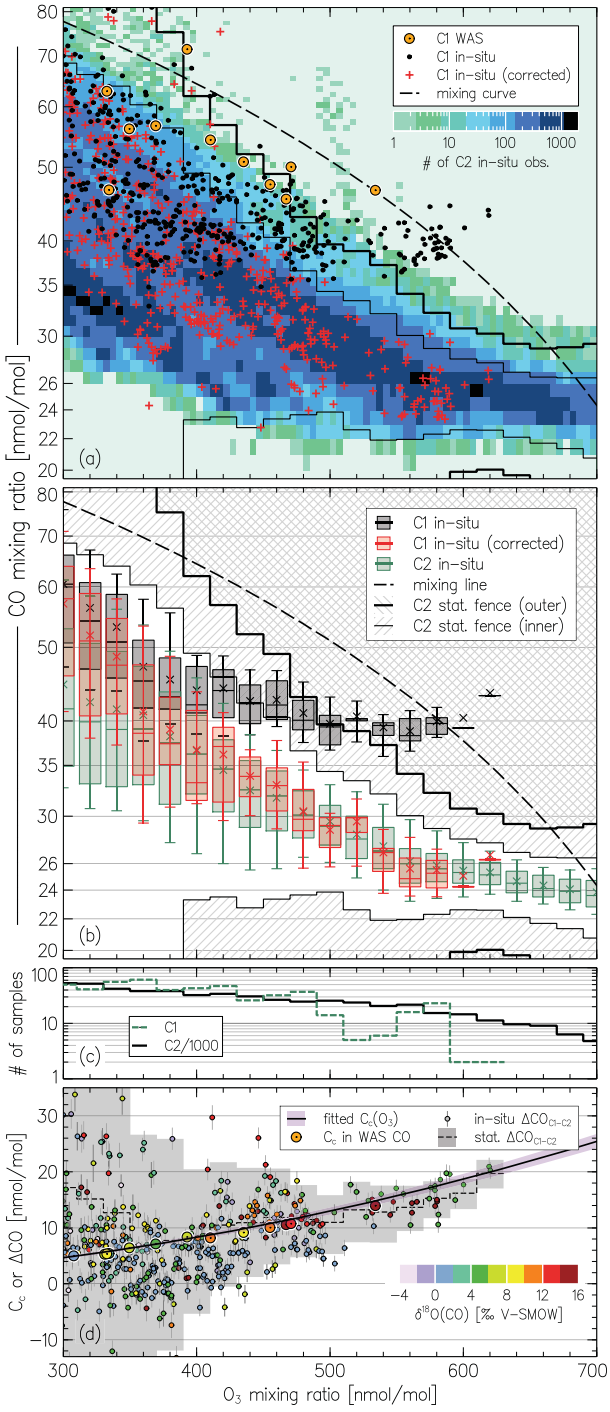
C1 WAS
C1 in-situ
C1 in-situ (corrected)
mixing curve
# of C2 in-situ obs.
(a)
C1 in-situ
C1 in-situ (corrected)
C2 in-situ
mixing line
C2 stat. fence (outer)
C2 stat. fence (inner)
(b)
CO mixing ratio [nmol/mol]
# of samples
C1
C2/1000
(c)
fitted $C_c(O_3)$
C_c in WAS CO
in-situ ΔCO_{C1-C2}
stat. ΔCO_{C1-C2}
$\delta^{18}O(CO)$ [‰ V-SMOW]
(d)
C_c or ΔCO [nmol/mol]
O_3 mixing ratio [nmol/mol]

Fig. 1. (a) Distribution of CO mixing ratios as a function of concomitant O_3 mixing ratios measured by CARIBIC in the LMS ([O_3]>300 nmol/mol). The shaded area is the two-dimensional histogram of the C2 measurements (all C2 data obtained until June 2013) counted in 5×1 nmol/mol size [O_3]×[CO] bins, thus darker areas emphasise greater numbers of particular CO−O_3 pairs observed. Small symbols denote the original C1 *in situ* measurements (black) and corrected for the artefacts (red); the C1 WAS analyses (11 of total 408) are shown with large symbols. Thin and thick step-lines demark the inner and outer statistical fences (ranges outside which the data points are considered mild or extreme outliers, see text) of the C2 data, respectively. The dashed curve exemplifies compositions expected from the linear mixing of very different (*e.g.*, tropospheric and stratospheric) end-members. (b) Statistics on CO mixing ratios from C1 and C2 data shown in box-and-whisker diagrams for samples clustered in 20 nmol/mol O_3 bins (whiskers represent $9^{th}/91^{st}$ percentiles). (c) Sample statistic for each CARIBIC dataset (note the C2 figures scaled down by a factor of 1000). (d) Estimates of the C1 *in situ* CO contamination strength C_c as a function of [O_3] (solid line) obtained by fitting the difference ΔCO between the C2 and C1 *in situ* [CO] (small symbols) in the kinetic framework (see Appendix A, Eq. (A1)). Step line shows the ΔCO for the statistical averages (the shaded area equals the height of the inner statistical fences of the C2 data). Large symbols denote the estimates of C_c in the C1 WAS data (slight variations *vs.* the *in situ* data are due to the sample mixing effects, see Sect. 3). Colour denotes the respective C1 WAS $\delta^{18}O(CO)$ (note that typically 6−7 *in situ* measurements correspond to one WAS sample).

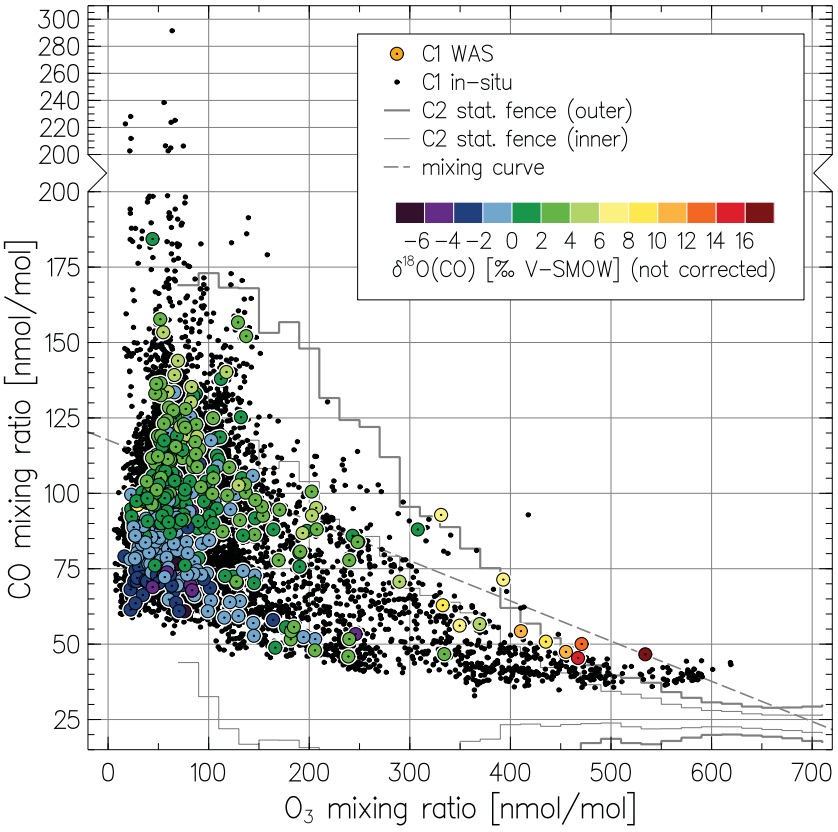

586 Fig. 2. (*accompanies Fig. 1*) Carbon monoxide and ozone mixing ratios measured in C1. Small black
587 symbols denote the C1 *in situ* measurements (n = 12753). The C1 WAS analyses (n = 408) are shown with
588 large symbols; colour denotes the concomitant $\delta^{18}O(CO)$ measurements. Thin and thick step-lines denote
589 the inner and outer statistical fences of the C2 data, respectively. The dashed curve exemplifies composi-
590 tions expected from the linear mixing of tropospheric and stratospheric end-members (see caption to Fig. 1
591 for details).

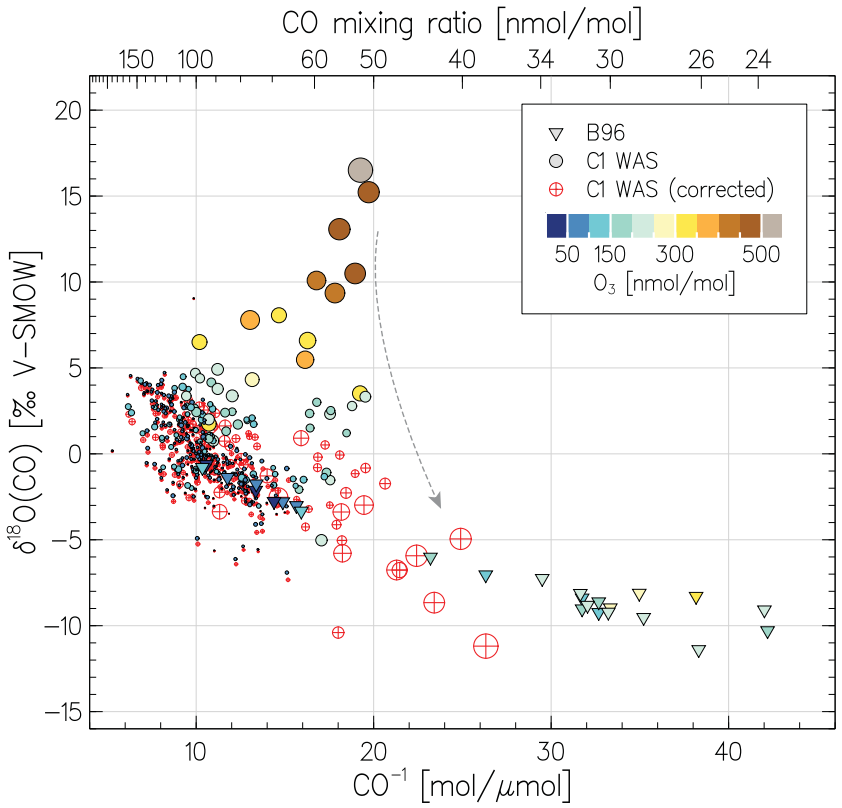

592 Fig. 3. $^{18}O/^{16}O$ isotope composition of CO as a function of its reciprocal mixing ratio. Triangles present
593 the data from the remote SH UT/LMS obtained by Brenninkmeijer *et al.* (1996) (B96). Colour refers to the
594 concomitantly observed O_3 abundances; note the extremely low [O_3] encountered by B96 in the Antarctic
595 "ozone hole" conditions. Filled and hollow circles denote the original and corrected (as exemplified by the
596 dashed arrow) C1 WAS data, respectively, with the symbol size scaling proportional to the estimated con-
597 tamination magnitude (see text).

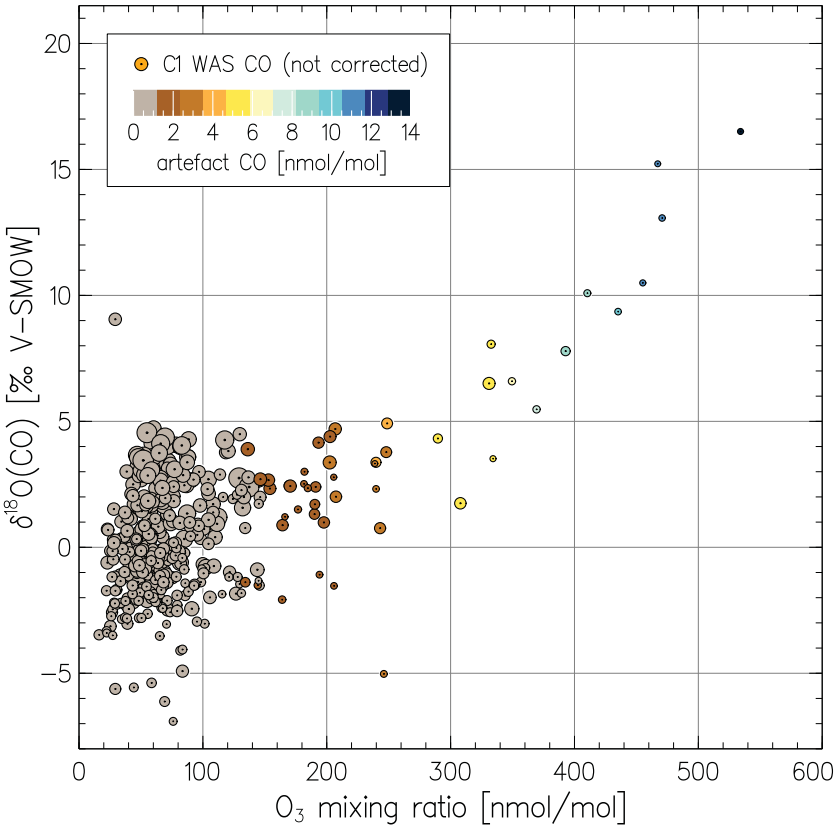

598 Fig. 4. Measured C1 WAS $\delta^{18}O(CO)$ (not corrected for artefacts) as a function of concomitant O_3 mixing
599 ratio. Symbol colour denotes the artefact CO component (integral C_c per each WAS); symbol size scales
600 proportionally to the WAS CO mixing ratio corrected for artefacts (see Sect. 3 for details).

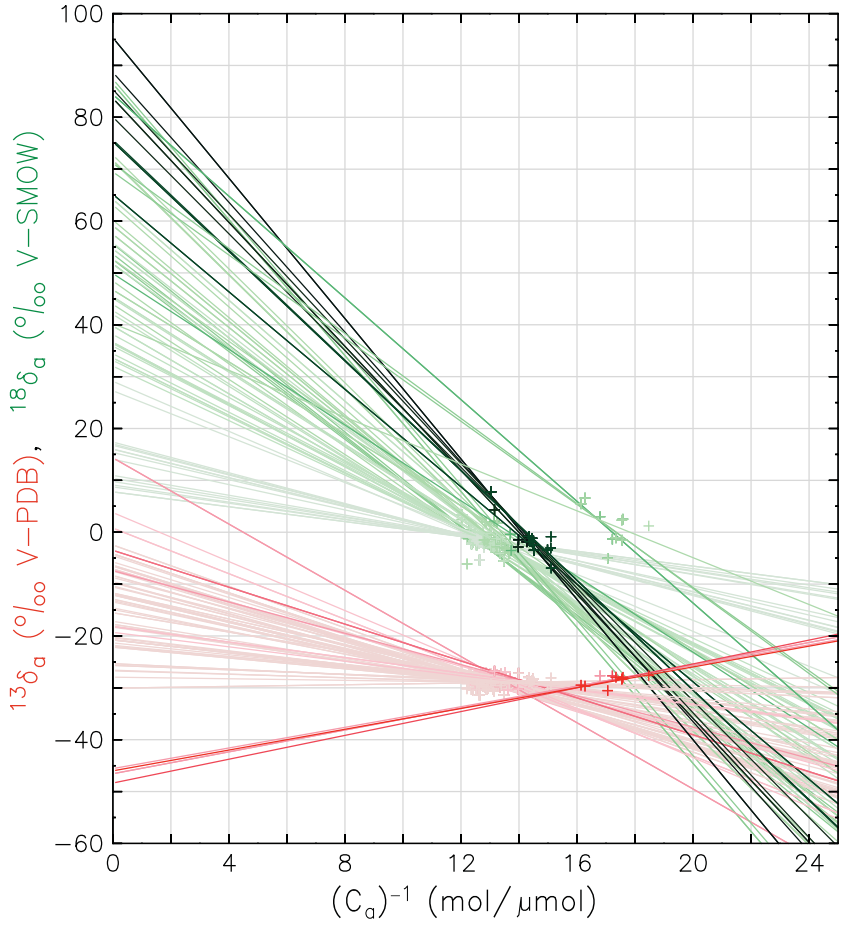

Fig. 5. Keeling plot of the data used in the calculations with the mixing model (MM). The C1 WAS isotope CO measurements are shown with symbols, solid lines denote the linear regressions through the various sets of samples selected by the MM (n = 80 sets are plotted). Colours refer to the $\delta^{13}C$ (red) and $\delta^{18}O$ (green) data, colour intensity indicates the coefficient of determination (R^2) of each regression, respectively. Darker colours denote higher R^2 values, with maxima of 0.92 for $\delta^{18}O$ and 0.54 for $\delta^{13}C$ data, respectively. The inferred contamination signatures (δ_c) are found at $(C_a)^{-1} \rightarrow 0$. Regression uncertainties are shown in Fig. 5. Note that because different subsets of samples contain same data points, some of the symbols are plotted over (*i.e.*, not all symbols contributing to a particular regression case may be seen).

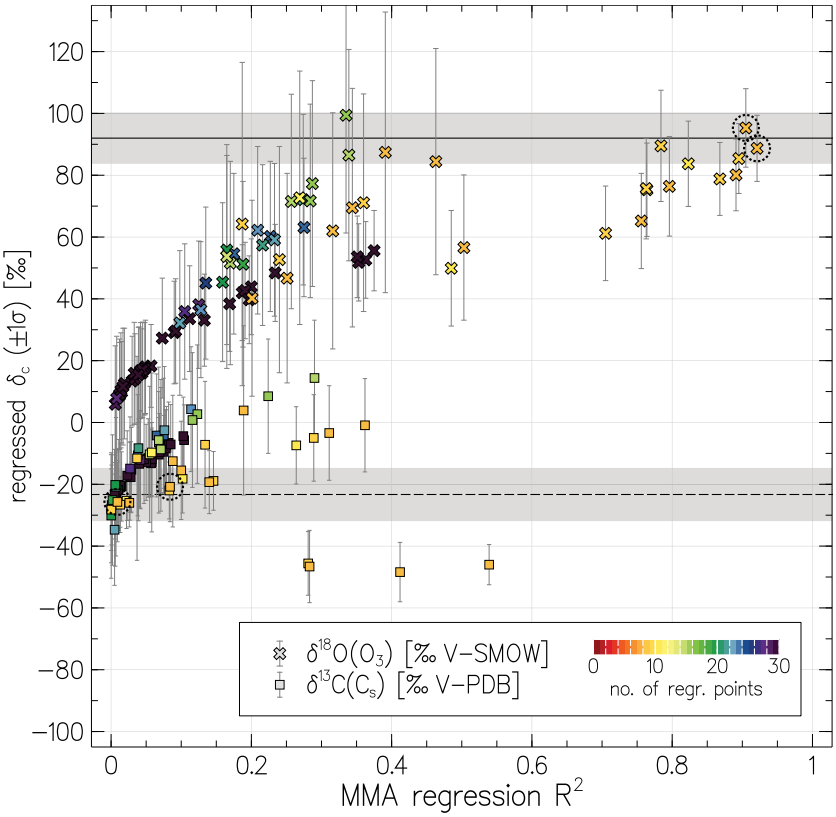

609 Fig. 6. Results of the regression calculation with the MM. Shown with symbols are the contamination
610 source isotope signatures δ_c as a function of the respective coefficient of determination (R^2). Colour de-
611 notes the number of samples in each subset selected. Solid and dashed lines present the best guess
612 ±1 standard deviation of the mean for the $\delta^{18}O(O_3)$ and $\delta^{13}C(C_c)$ estimates. Dashed circles mark the values
613 obtained at highest R^2 for $^{18}O\delta_t$ regression (above 0.9). See text for details.

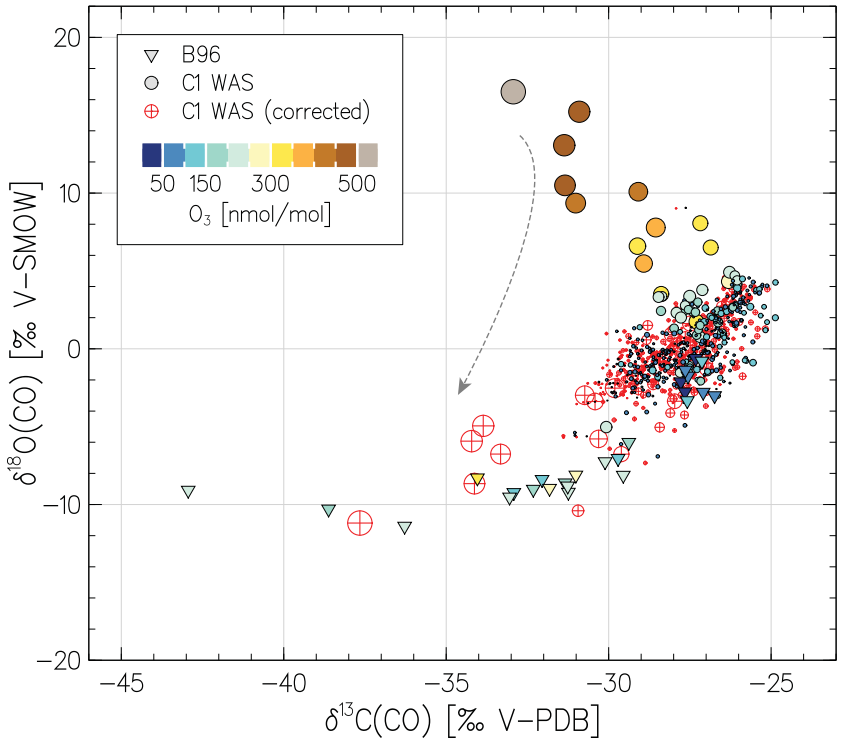

Fig. 7. $^{18}O/^{16}O$ and $^{13}C/^{12}C$ isotope composition of CO measured in C1. Triangles present the data from the remote SH UT/LMS obtained by Brenninkmeijer *et al.* (1996) (B96). Colour refers to the concomitantly observed O_3 abundances; note the extremely low [O_3] encountered by B96 in the Antarctic ozone-hole conditions. Filled and hollow circles denote the original and corrected (as exemplified by the dashed arrow) C1 WAS data, respectively, with the symbol size scaling proportional to the estimated contamination magnitude (see text for details).